Journal of Circuits, Systems, and Computers
Vol. 22, No. 2 (2013) 1250078 (18 pages)

DOI: 10.1142/S0218126612500788

RECURSIVE QR DECOMPOSITION ARCHITECTURE FOR MIMO-OFDM DETECTION SYSTEMS*

ROBERT CHEN-HAO CHANG† and HUNG-LIEH CHEN

Department of Electrical Engineering,
National Chung-Hsing University,
250 Kuo Kuang Rd.,
Taichung 402, Taiwan

National Chip Implementation Center,
National Applied Research Laboratories,
Hsinchu, Taiwan
†*chchang@dragon.nchu.edu.tw*

KUANG-HAO LIN‡

Department of Electronic Engineering,
National Chin-Yi University of Technology,
57 Sec. 2 Zhongshan Rd., Taiping Dist.,
Taichung 411, Taiwan
khlin@ncut.edu.tw

MING-FAN WEI

Department of Electrical Engineering,
National Chung-Hsing University,
250 Kuo Kuang Rd., Taichung 402, Taiwan
mingfan.wei@gmail.com

Received 19 April 2011
Accepted 19 March 2012
Published 6 March 2013

This paper presents a modified implementation of QR decomposition for multiple input multiple output-orthogonal frequency division multiplexing (MIMO-OFDM) detection based on the Givens rotation method. The QR decomposition hardware is constructed using the coordinate rotation digital computer (CORDIC) algorithm operating with fewer gate counts and lower power consumption than do triangular systolic array (TSA) structures. Accurate signal transmission is essential to wireless communication systems. Thus, a more effective data detection algorithm and precise channel estimation method play vital roles in MIMO systems. Implementing data detection with QR decomposition helps reduce the complexity of MIMO-OFDM detection. Implementation results reveal that the proposed recursive QR decomposition

*This paper was recommended by Regional Editor Eby G. Friedman.
‡Corresponding author.

(RQRD) architecture has lower clock latency than do TSA structures, and has a smaller hardware area than do Gram−Schmidt structures.

Keywords: QR decomposition; MIMO-OFDM; detection; CORDIC; architecture.

1. Introduction

A recent surge of research on wireless local area networks (WLANs) has generated new challenges and opportunities. With the increasing use of wireless communication systems, reliability requirements for high data rates have become more critical. In view of this, the IEEE 802.11n system is based on multiple input multiple output (MIMO)-orthogonal frequency division multiplexing (OFDM) technology.[1−3] The advantages of MIMO-OFDM are that it uses bandwidth more efficiently and combats the inter-symbol interference (ISI) effect and multi-path effect. Therefore, the current trend in WLAN development is to use MIMO-OFDM technology.

The detection algorithm technique for MIMO-OFDM wireless communication systems increases spectral efficiency.[4−7] However, its complex receiver makes it unsuitable for low-complexity very-large-scale integration (VLSI) implementation. Researchers have proposed several alternative algorithms and architectures to reduce the complexity of this detection.[8,9] Lai *et al.*[8] proposed a low-complexity adaptive tree search algorithm for MIMO detection. In that design, an algorithm adapting the number of partitions based on the channel conditions is presented to achieve a more favorable tradeoff between complexity and performance. Sobhanmanesh *et al.*[9] offered a nearly optimal algorithm for V-BLAST detection in MIMO wireless communication systems based on QR factorization. In that approach, however, an efficient implementation of the detection requires QR decomposition to reduce the hardware complexity of the MIMO-OFDM receiver.

Related studies on the QR decomposition architecture can be classified into two major hardware implementation categories. The first category is a parallel architecture based on the modified Gram−Schmidt (MGS) algorithm.[10,11] The second category is the triangular systolic array (TSA), based on the coordinate rotation digital computer (CORDIC) algorithm.[12,13] However, based on extensive literature regarding QR decomposition, relatively few studies have focused on the relationship between clock latency and hardware area.

This paper proposes a recursive QR decomposition (RQRD) hardware architecture based on the Givens rotation method for MIMO-OFDM detection systems. From a hardware perspective, the RQRD method is constructed using the CORDIC algorithm, which has a lower gate count and clock latency than do TSA structures. The QR decomposition architecture uses an iteration operation to reduce hardware complexity via a vectoring mode and rotating mode circuits. Simulation results demonstrate the performance of QR decomposition at various iteration numbers.

The remainder of this paper is organized as follows. Section 2 describes the MIMO-OFDM detection systems. Section 3 introduces the QR decomposition algorithm. Section 4, presents the efficient QR decomposition architecture. In Sec. 5, the simulation and implementation results are presented. Finally, conclusions are drawn in Sec. 6.

2. MIMO-OFDM Detection Systems

2.1. *System block diagram*

To increase the data rate of wireless communications, a MIMO system uses the spatial multiplex with Nt transmitted antennas and Nr received antennas. The block diagram of the MIMO-OFDM system is shown in Fig. 1. The source data passes through modulation, spatial time coding, and inverse fast Fourier transform and cyclic prefix (IFFT/CP) to transmit antennas in the transmitter. The receiver site includes fast Fourier transform and removed cyclic prefix (ReCP/FFT), channel estimation, QR decomposition, spatial multiplex detection, and demodulation to restore the source data.

The main functionality of an OFDM system is to address the frequency selection effect. The receiver block diagram shown in Fig. 1, the received signals at the kth subcarrier $\mathbf{Y}_k = [y_1(t), y_2(t), \ldots, y_{Nr}(t)]^{\mathrm{T}}$ can be obtained in the frequency domain, as Eq. (1) indicates

$$\mathbf{Y}_k = \mathbf{H}_k \mathbf{X}_k + \mathbf{n}_k\,, \quad \text{for } k = 1, 2, \ldots, Nc\,, \tag{1}$$

where $\mathbf{X}_k = [x_1(t), x_2(t), \ldots, x_{Nt}(t)]^{\mathrm{T}}$ is the transmitter signal, $\mathbf{H}_k$ denotes the channel response, $\mathbf{n}_k$ denotes the additive white Gaussian noise (AWGN), and Nc denotes the subcarrier number. Equation (1) represents a MIMO system with Nt transmitted antennas and Nr received antennas. The QR decomposition of $\mathbf{H}_k$ is

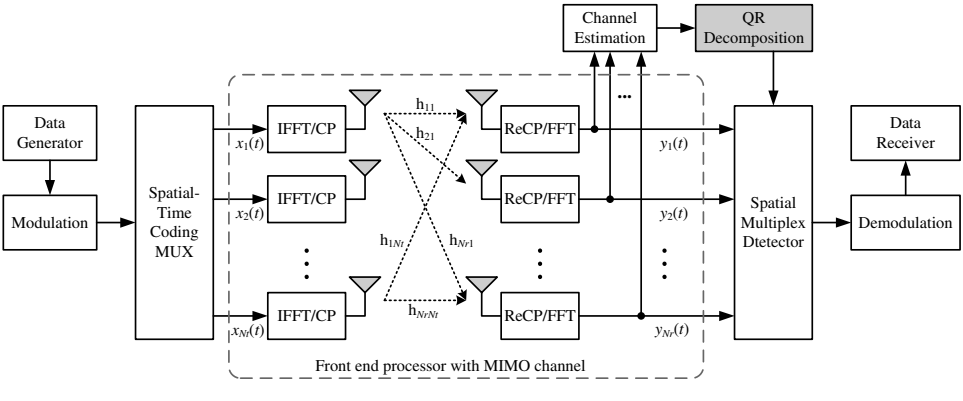

Fig. 1. Block diagram of a spatial multiplex MIMO-OFDM wireless communication system.

derived from the known preambles or known training sequences of the wireless communication system, according to the channel estimation in Fig. 1.[14]

2.2. *MIMO detection*

Detecting the joint QR decomposition and partial sphere decoder (JQRPSD) method has six discrete steps[15]: radius constraint of the sphere, successive cancellation detection (SCD), QR decomposition, slicer, tree pruning, and min-search.

QR decomposition uses the pre-processor to process the channel response $\mathbf{H}$ first, and then decomposes it into $\mathbf{Q}$ and $\mathbf{R}$ matrices to produce $\mathbf{H} = \mathbf{QR}$. Hereafter, the subcarrier index k is omitted for the sake of simplicity. The detected vector $\hat{\mathbf{s}}$ is computed based on the maximum likelihood (ML) algorithm with QR decomposition, as given in Eq. (2)

$$\begin{aligned}\hat{\mathbf{s}} &= \arg\min \|\mathbf{Y} - \mathbf{HX}\|^2 = \arg\min \|\mathbf{Q}^H\mathbf{Y} - \mathbf{RX}\|^2 \\ &= \arg\min \|\hat{\mathbf{y}} - \mathbf{RX}\|^2, \end{aligned} \tag{2}$$

where $\mathbf{Q}$ denotes an $Nr \times Nt$ orthogonal matrix and $\mathbf{R}$ represents an upper triangular matrix.

The received signal $\mathbf{Y}$ in Eq. (1) can be modified using $\mathbf{Q^H}$ to obtain

$$\begin{aligned}\hat{\mathbf{y}} &= [\,\hat{y}_1 \quad \cdots \quad \hat{y}_{Nr-1} \quad \hat{y}_{Nr}\,]^{\mathrm{T}} = \mathbf{Q}^H\mathbf{Y} \\ &= \mathbf{Q}^H\mathbf{QRX} + \mathbf{Q}^H\mathbf{n} = \mathbf{RX} + \mathbf{Q}^H\mathbf{n} \\ &= \begin{bmatrix} r_{1,1} & \cdots & r_{1,Nr-1} & r_{1,Nr} \\ 0 & \ddots & \vdots & \vdots \\ \vdots & & r_{Nr-1,Nr-1} & r_{Nr-1,Nr} \\ 0 & \cdots & 0 & r_{Nr,Nr} \end{bmatrix} \begin{bmatrix} x_1 \\ \vdots \\ x_{Nr-1} \\ x_{Nr} \end{bmatrix} + \begin{bmatrix} n_1 \\ \vdots \\ n_{Nr-1} \\ n_{Nr} \end{bmatrix}. \end{aligned} \tag{3}$$

3. QR Decomposition Algorithm

Most modern MIMO-OFDM data-detection methods include the QR decomposition algorithm. The primary reason for this is that, after QR decomposing of the channel response, the data can remain orthogonal and signal processing can thus be simplified. When the channel response H is QR decomposed, it is transformed into an up-triangular matrix R. This effectively reduces the interference of every signal received. Because using the QR decomposition algorithm can decrease equalizer complexity, the additional QR decomposition does not increase the total size.

Common QR decomposition algorithms are the Gram−Schmidt orthogonalization, Givens rotation, and Householder transformation.[16] Because Householder transformation is much more complex in hardware implementation than the other

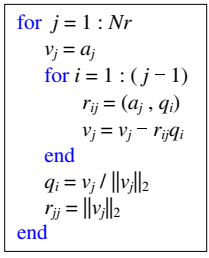

Fig. 2. Gram−Schmidt orthogonalization algorithm.

two algorithms, this paper discusses only the Gram−Schmidt orthogonalization and the Givens rotation.

3.1. *Gram−Schmidt*

The QRD for any matrix can be realized using the Gram−Schmidt orthogonalization algorithm.[17] This procedure reduces the memory hardware consumption. The Gram−Schmidt orthogonalization algorithm is shown in Fig. 2.

a_{ij} denotes row i and column j of the matrix $\mathbf{A}$, and $\mathbf{a}_i$ denotes the column vector of the matrix $\mathbf{A}$. For simplicity, the 3×3 matrix $\mathbf{A}$ is utilized to explain the procedure. The QRD of matrix $\mathbf{A}_{3\times3}$, $\mathbf{A}_{3\times3} = \mathbf{Q}_{3\times3}\mathbf{R}_{3\times3}$, can be obtained using the Gram−Schmidt orthogonalization algorithm,[10] in which

$$\mathbf{A} = \begin{bmatrix} a_{11} & a_{12} & a_{13} \\ a_{21} & a_{22} & a_{23} \\ a_{31} & a_{32} & a_{33} \end{bmatrix}, \quad \mathbf{Q} = \begin{bmatrix} q_{11} & q_{12} & q_{13} \\ q_{21} & q_{22} & q_{23} \\ q_{31} & q_{32} & q_{33} \end{bmatrix}, \quad \mathbf{R} = \begin{bmatrix} r_{11} & r_{12} & r_{13} \\ 0 & r_{22} & r_{23} \\ 0 & 0 & r_{33} \end{bmatrix}.$$

3.2. *Givens rotation*

The Givens rotation rotates in the plane expended by two coordinate axes. The rotation matrix can be expressed as

$$\mathbf{G}(m, n, \theta) = \begin{bmatrix} 1 & \cdots & 0 & \cdots & 0 & \cdots & 0 \\ \vdots & \ddots & \vdots & & \vdots & & \vdots \\ 0 & \cdots & \cos\theta_{m,m} & \cdots & -\sin\theta_{m,n} & \cdots & 0 \\ \vdots & & \vdots & \ddots & \vdots & & \vdots \\ 0 & \cdots & \sin\theta_{n,m} & \cdots & \cos\theta_{n,n} & \cdots & 0 \\ \vdots & & \vdots & & \vdots & \ddots & \vdots \\ 0 & \cdots & 0 & \cdots & 0 & \cdots & 1 \end{bmatrix}. \tag{4}$$

Here, $\mathbf{G}(m,n,\theta)^{\mathrm{T}} \cdot \mathrm{X}$ denotes that vector X rotates counterclockwise an angle θ in the (m,n) plane. When the rotation matrix G multiplies another matrix A, it only affects the ith and kth rows of matrix A.

Given a non-singular $n \times n$ matrix $\mathbf{A}$, we use a Givens rotation to obtain QR factorization of $\mathbf{A}$. Let $\mathbf{G}_{21}$ be the Givens rotation acting on the 1st and 2nd coordinates so that a zero results in the (2, 1) position. We can apply another Givens rotation $\mathbf{G}_{31}$ to $(\mathbf{G}_{21} \cdot \mathbf{A})$ to obtain a zero in the (3, 1) position. The process can be continued until the final $n-1$ entries in the first column have been eliminated.

$$\mathbf{G}_{n1} \cdots \mathbf{G}_{31}\mathbf{G}_{21}\mathbf{A} = \begin{bmatrix} \times & \times & \cdots & \times \\ 0 & \times & \cdots & \times \\ 0 & \times & \cdots & \times \\ \vdots & & & \\ 0 & \times & \cdots & \times \end{bmatrix}. \tag{5}$$

Next, Givens rotation $\mathbf{G}_{32}, \mathbf{G}_{42}, \ldots, \mathbf{G}_{n2}$ are used to eliminate the last $n-2$ entries in the 2nd column. This process is continued until all elements below the diagonal have been eliminated.

$$(\mathbf{G}_{n,n-1}) \cdots (\mathbf{G}_{n2} \cdots \mathbf{G}_{32})(\mathbf{G}_{n1} \cdots \mathbf{G}_{21})\mathbf{A} = \mathbf{R}, \tag{6}$$

where $\mathbf{R}$ is an upper triangular matrix. If we let $\mathbf{Q}^{\mathrm{T}} = (\mathbf{G}_{n,n-1}) \cdots (\mathbf{G}_{n2} \cdots \mathbf{G}_{32})(\mathbf{G}_{n1} \cdots \mathbf{G}_{21})$, then $\mathbf{A} = \mathbf{QR}$ and $\mathbf{A}\boldsymbol{x} = \mathbf{b}$ is equivalent to $\mathbf{Rx} = \mathbf{Q}^{\mathrm{T}}\mathbf{b}$.

Therefore, the rotation matrix G can be simplified as

$$\mathbf{G} = \begin{bmatrix} \cos\theta & -\sin\theta \\ \sin\theta & \cos\theta \end{bmatrix}. \tag{7}$$

The mathematical form can be expressed as

$$\begin{bmatrix} \cos\theta & -\sin\theta \\ \sin\theta & \cos\theta \end{bmatrix} \begin{bmatrix} \alpha \\ \beta \end{bmatrix} = \begin{bmatrix} \gamma \\ 0 \end{bmatrix}, \tag{8}$$

where $\gamma = \sqrt{(\alpha)^2 + (\beta)^2}$, $\cos\theta = \alpha/\gamma$, $\sin\theta = -\beta/\gamma$. The rotation matrix G value can be obtained from r.

Based on Eq. (8), if QR decomposition is to be executed on any matrix, an up-triangular matrix R can be obtained only through successive multiplication of the rotation matrix G. The orthogonal matrix Q can also be obtained by executing the same operation on identity matrix I. When the QR decomposition is achieved using the Givens rotation method, the hardware complexity can be reduced using the CORDIC operation core with vectoring and rotating modes.

QR decomposition enables using the CORDIC vectoring mode to convert the complex input matrix numbers into real numbers and perform row cancellation. This produces the R matrix of QR (an up-triangular matrix, all of whose diagonal elements are real numbers). Mathematically, assume that the input is equal to $\alpha + i\beta$,

and use the CORDIC vectoring mode to eliminate β. In other words, use each calculated value β to control the direction of rotation. The vectoring equation is determined using

$$\begin{cases} \alpha_{p+1} = \alpha_p - \beta_p \cdot d_p \cdot 2^{-p} \\ \beta_{p+1} = \beta_p + \alpha_p \cdot d_p \cdot 2^{-p} \\ \theta_{p+1} = \theta_p + d_p \cdot \tan^{-1}(2^{-p}) \end{cases} \quad \text{where} \begin{cases} d_p = 1\,, & \beta_p < 0\,, \\ d_p = -1\,, & \text{otherwise}\,. \end{cases} \tag{9}$$

After pth iterations, we can obtain $\beta = 0$, and new coordinates $(\alpha', 0)$ with a rotational angle θ.

The rotating mode causes a coordinate to rotate at a given angle or cause two coordinates to rotate at the same angle. For QR decomposition, the rotating angle θ produced using the vectoring mode is transmitted to other elements of the same row for coordinate rotation. The direction of rotation can be controlled for every calculated value of θ. The rotating equation is determined using

$$\begin{cases} \alpha_{p+1} = \alpha_p - \beta_p \cdot d_p \cdot 2^{-p} \\ \beta_{p+1} = \beta_p + \alpha_p \cdot d_p \cdot 2^{-p} \\ \theta_{p+1} = \theta_p - d_p \cdot 2^{-p} \end{cases} \quad \text{where} \begin{cases} d_p = -1\,, & \theta_p < 0\,, \\ d_p = 1\,, & \text{otherwise}\,. \end{cases} \tag{10}$$

After pth iterations, we can obtain $\theta = 0$ and new coordinates $(\alpha'\beta')$, which is the result of rotating the angle θ. Both the vectoring mode and rotating mode have a maximum angle restriction, and the range is $-\pi/2 \sim \pi/2$. If the angle exceeds the maximum value that $\tan\theta$ can represent, it may produce an inaccurate calculation. Therefore, it is necessary to rotate the coordinates on the second and third quadrants to the first and fourth quadrants using Eq. (11):

$$\underbrace{\begin{array}{l} d_0 = -\text{sign}(\beta_0) \\ \alpha_{\text{initial}} = -d_0 \cdot \beta_0 \\ \beta_{\text{initial}} = d_0 \cdot \alpha_0 \\ \theta_{\text{initial}} = d_0 \cdot \pi/2 \end{array}}_{\text{Vectoring Mode}} , \quad \underbrace{\begin{array}{l} d_0 = \text{sign}(\theta_0) \\ \alpha_{\text{initial}} = -d_0 \cdot \beta_0 \\ \beta_{\text{initial}} = d_0 \cdot \alpha_0 \\ \theta_{\text{initial}} = \theta_0 - d_0 \cdot \pi/2 \end{array}}_{\text{Rotationg Mode}} \tag{11}$$

where α_0, β_0, θ_0, are the input values.

3.3. *Composition scheme*

Using Gram−Schmidt orthogonalization for hardware implementation requires more complicated hardware[11] including complex number multipliers, square roots, and dividers. The Givens rotation is based on the CORDIC algorithm, which simply consists of adding and shifting. However, Givens rotation cancellation separates the operation of the real part from the imaginary part. This Givens rotation scheme increases the hardware size, and the control signal is considerably more complicated. This sub-section first addresses the estimated channel response H using Eq. (12), and

then converts the channel response H from a complex matrix into a real symmetric matrix.

$$\mathbf{H} = \begin{bmatrix} h_{11} & \cdots & h_{1,N_r} \\ \vdots & \ddots & \vdots \\ h_{N_r,1} & \cdots & h_{N_r,N_r} \end{bmatrix} \Rightarrow \mathbf{H}' = \begin{bmatrix} \mathrm{Re(H)} & -\mathrm{Imag(H)} \\ \mathrm{Imag(H)} & \mathrm{Re(H)} \end{bmatrix}. \tag{12}$$

Based on Eq. (12), we can perform matrix cancellation using the Givens rotation. Furthermore, we can also change the sequence of matrix operations. For example, when performing the first row cancellation, all of the cancellations are executed by the first row. The algorithm of cancellation is depicted in Fig. 3, where $(\,)^*$ denotes the Hermitian operator.

Row cancellation includes vectoring computing and rotating computing which can eliminate an element $(h_{2,1})$ of the matrix row and adjust angles of the other elements $(h_{2,2}, \ldots, h_{2,2Nr})$, respectively, as Fig. 3 shows. Employing the same cancellation process for the element $(h_{2,1})$, the elements $(h_{3,1}, \ldots, h_{Nr,1})$ can be eliminated by the first row. Regarding the aforementioned methods, the algorithm of cancellation process is repeated until the final process of elimination for QR decomposition. The matrix $\mathbf{R}$ can then be obtained as

$$\mathbf{R} = \begin{bmatrix} r_{11} & r_{12} & \cdots & r_{1,2N_r} \\ 0 & r_{22} & \cdots & \vdots \\ \vdots & \ddots & \ddots & r_{2N_r-1,2N_r} \\ 0 & \cdots & 0 & r_{2N_r,2N_r} \end{bmatrix}.$$

Because we separate the real part from the imaginary part of the matrix using this QR decomposition, it may cause matrix expansion ($m = 2Nr$, Nr is the dimension of the original matrix $\mathbf{H}$). Furthermore, the results of each operation step of QR decomposition are placed into storage units, increasing the circuit area. However, adopting the CORDIC structure processing unit instead of the Gram−Schmidt orthogonalization structure can decrease the circuit area. In our circuit

```
for m = 1:2N_r - 1
  for n = m+1:2N_r
    G̃_{2N_r x 2N_r} = G_{2N_r x 2N_r}(m,n)
    H'_{2N_r x 2N_r} = G̃_{2N_r x 2N_r} · H'_{2N_r x 2N_r}
    Q*_{2N_r x 2N_r} = G̃_{2N_r x 2N_r} · I_{2N_r x 2N_r}
  end
end
```

Fig. 3. Algorithm of cancellation process for QR decomposition.

implementation, using Register File rather than SRAM as storage units can also greatly decrease the hardware area. In brief, with the proposed RQRD, CORDIC and Register File, the circuit area does not increase excessively because of matrix expansion. The detailed circuit design is discussed in the following section.

4. Hardware Architecture Design

The hardware architecture design of QR decomposition is extensively discussed in current MIMO-OFDM detection system studies on enhancing operational efficiency. The most popular architecture adopted is the TSA with processing elements based on CORDIC computing.

4.1. *Systolic array*

The TSA consists of a set of processing units. Each processing unit can perform simple operations. The advantages of this architecture are a simple and regular design that can accelerate computation flow. Figure 4 shows the TSA architecture for QR decomposition. Using the TSA architecture for QR decomposition, the hardware can offer high throughput; but the processing units increase as the dimension of H increases. The special method of folding architecture, which requires a small processor, was developed by a previous.[9] Unfortunately, this approach requires longer clock latency and more memory.

The TSA method of QR decomposition can efficiently separate MIMO-OFDM channel information to up triangular matrix **R** and orthogonal matrix **Q**. Figure 5 shows the schedule of operations for a 2×2 MIMO-OFDM channel effect ($N = 2$, $h_{11} \sim h_{44}$), where the circle denotes the vectoring operation, the square denotes the rotating operation, and $Y_1 \sim Y_4$ are receiver signals. The TSA processing in this case requires 12 time slots from T_1 to T_{12}, which can be formulated as $2\sum_{i=1}^{m-1}(m-i)$, where m denotes the matrix order. Each time slot has p-clock operations, where p is

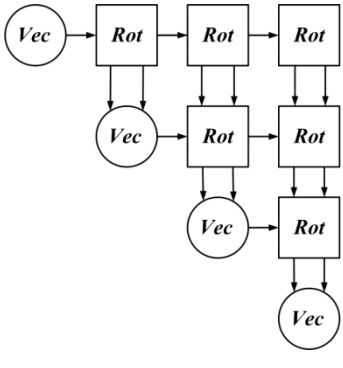

Fig. 4. Architecture of TSA for QR decomposition.

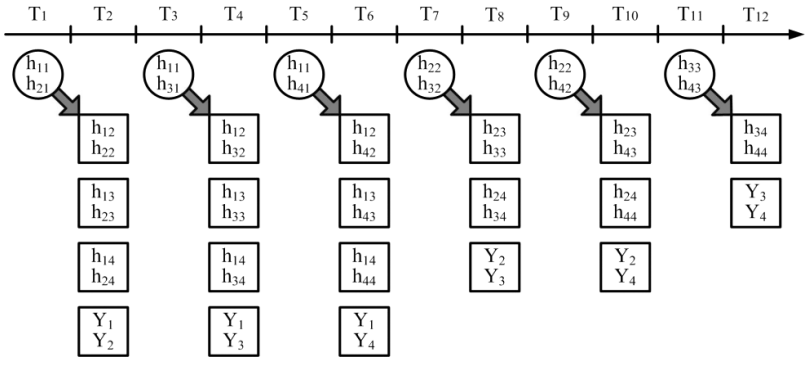

Fig. 5. QR decomposition processing scheme for 2×2 MIMO-OFDM channel information.

defined according to the vectoring or rotating iteration times. Therefore, the clock latency is computed as $2p\sum_{i=1}^{m-1}(m-i) = 2 \times 8 \times 6 = 96$ clocks, where iteration is denoted eight times, and matrix order m equals 4. The hardware area is defined as $A_{\text{Vec}}m + A_{\text{Rot}}\sum_{i=1}^{m-1}(m-i)$ gate counts, where the A_{Vec} is a vectoring hardware area and A_{Rot} is a rotating hardware area.

4.2. *Recursive QR decomposition*

This paper proposes the RQRD architecture shown in Fig. 6. This architecture increases CORDIC processing units, according to matrix expansion, but requires neither a complex control circuit nor rotating mode circuit. Thus, the area of a single CORDIC processing unit is smaller than that of the architecture introduced previously. The registers (Reg) are used as a storage unit. The register size is m^2, according to matrix order. Every processing unit requires a register circuit, but these can be shared with the previous stage, thereby minimizing the hardware size of the receiver. The RQRD structure is proposed, based on TSA to reduce complexity and hardware area, which can be defined as $A_{\text{Vec}} + A_{\text{Rot}}(m-1)$ gate counts. Compared

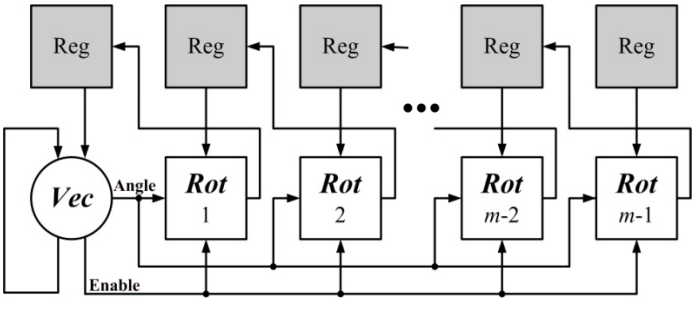

Fig. 6. RQRD architecture.

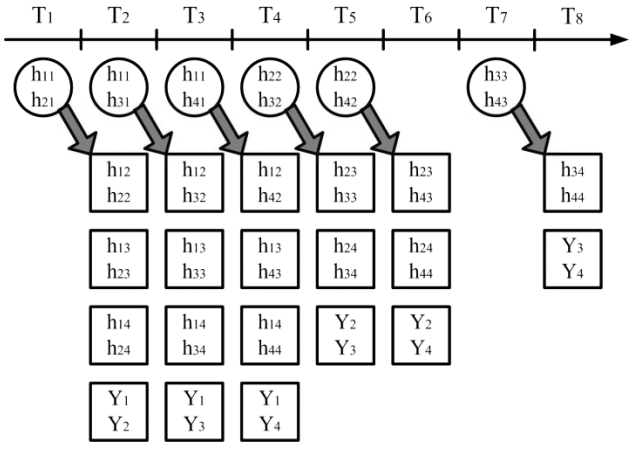

Fig. 7. QR decomposition processing scheme for 2×2 MIMO-OFDM channel information.

with the TSA, RQRD hardware can decrease $A_{\text{Vec}}(m-1) + A_{\text{Rot}} \sum_{i=2}^{m-1}(m-i)$ gate counts. The RQRD processing employs time-constrained scheduling to decrease the operation time, as Fig. 7 shows. Therefore, the clock latency can be formulated as $p(2 + \sum_{i=1}^{m-1}(m-i))$, and the QR decomposition processing for 2×2 MIMO-OFDM requires 64 clocks, where $m = 4$ and $p = 8$.

Because each CORDIC processing unit works independently, the vectoring mode register must be dual-port to avoid the two processing units, vectoring mode, and rotating mode from reading or writing the first register simultaneously, which may lead to inaccurate calculation. The vectoring mode and rotating mode are originally dual-input processing units. Here, we modify them to be single-input, with the output feedback as the next input. After the first operation, an enabling signal and a rotational angle are sent to the rotating mode to begin the operation. At this moment, the enabling signal stimulates the vector mode to read the next register address data, and then continues to perform subsequent operations until it receives the disable signal from the control circuit.

The architecture of the control circuit is simpler because it is not necessary to determine whether or not to convert the real part or the imaginary part. A vectoring mode control circuit uses two counters (i.e., one upper counter and one lower counter. The upper counter is controlled by processing units). When the vectoring mode acquires its result, it sends an enabling signal to the next stage. At that precise instant, the register is stimulated to read and process the next row of matrix elements. The lower counter is an index counter, whose value is counted down from m, where m is the matrix order. When the values of the upper counter and the lower counter become identical, the lower counter subtracts 1, and the first row operation result is sent out. The second row vector cancellation proceeds as normal. The QR

decomposition operation ends when the values of the upper counter and lower counter are both 2 simultaneously.

Control circuits for the rotating mode and vectoring mode share a similar design concept. The only difference is that the stimulating signal is sent after the operation of the rotating mode circuit. Simultaneously, the enabling signal stimulates the final stage of the register and writes the rotating data into the register. Each rotating mode processing unit works independently, but is synchronized. Therefore, all of the rotating mode processing units can share the same control circuit.

4.3. *Vectoring and rotation*

The vectoring mode and rotating mode also share similar design concepts for finite state machines (FSM). The only difference is that the principles the two operations use to determine directions vary. Before outputting the operation results, the rotating mode must correct one more value than the vectoring mode does.

The following section first introduces the function of each state of the FSM from ST0 to ST4. Figure 8 shows a detailed flow chart of the state machine, where the *Rst* denotes the reset signal, the *En* denotes the enabling signal, and the *End_FSM* denotes the FSM operation finish signal.

ST 0: Reset (*Rst*) all values to zero. All circuits remain stopped until they receive an enabling signal (*En*) from the previous stage and jump to State 1 and begin working.

ST 1: After the register loads the values, they are sent to the vectoring/rotating mode for execution. The values on the second and third quadrants are first converted to calculable values on the first and fourth quadrants, setting the rotation angle within $180°(+90° \text{ to } -90°)$.

ST 2: The desired operational values are substituted into the equations for iteration. After p iterations, the result converges and jumps to State 3. For circuit implementation, we use a counter to calculate the number of iterations.

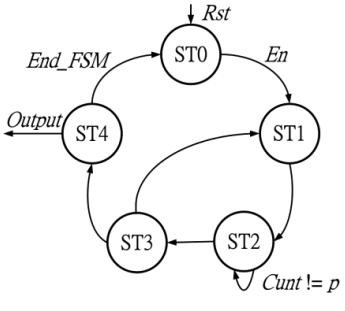

Fig. 8. Vectoring/rotating mode state machine.

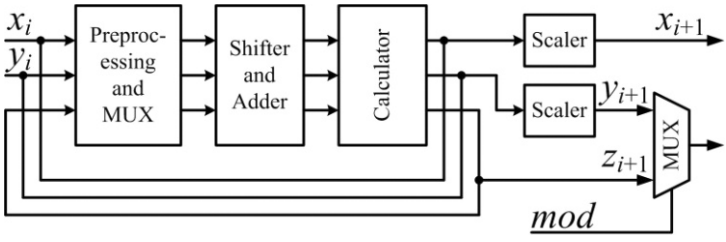

Fig. 9. Vectoring mode and rotating mode architecture.

Therefore, if the counter value *Cunt* is not equal to p ($Cunt\,! = p$), then the state would remain in this state.

ST 3: The calculated value from State 2 is not the true value and must be corrected by multiplying it by a scale factor. The corrected value is then the true value.

ST 4: The system determines whether or not row cancellation is complete. If it is complete, the values of the row vector would be exported. Otherwise, the system jumps back to State 0 and continues to finish the row cancellation. When complete, this step sends out an enabling signal (*End_FSM*) to inform the next stage to begin operation.

The desired input rotational angle of the rotating mode is obtained from the calculation result of vectoring mode. When the vectoring mode operation creates a result, the system must generate an enabling signal and, combined with the calculated angle, send it to the rotating mode operation. When the rotating mode receives the enabling signal, it begins to operate. An enabling signal is generated after the rotation mode operation. This signal is used to begin register storing. The calculated results of the rotating mode are then written into the register. Figure 9 shows the architecture of the vectoring mode and rotating mode. The vectoring and rotating mode with output signal z_{i+1} and y_{i+1}, respectively, can be selected using the *mod* signal.

5. Simulation and Implementation Results

The simulations of the vectoring mode and rotating mode of CORDIC algorithm are simulated by Matlab. Figure 10 shows the converging curve characteristics of the vectoring mode. The initial value is (1, 1). After iteration with the vectoring mode equation, the result is (1.4142, 0) and the angle to rotate $z = (-\pi/4)$. In Fig. 11, the initial value is (1, 1) and the angle to rotate is π. After iteration with the rotating mode equation, the result is $(-1, -1)$ and the angle to rotate is 0. The simulation results show that the converging speed of CORDIC algorithm is extremely fast and the number of iterations is 6−8. The output value, therefore, is stable and remains unchanged.

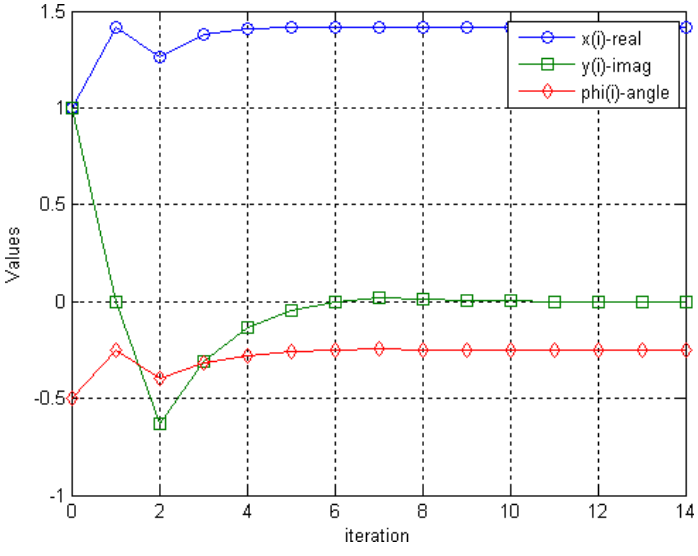

Fig. 10. Convergence curve of vectoring mode (color online).

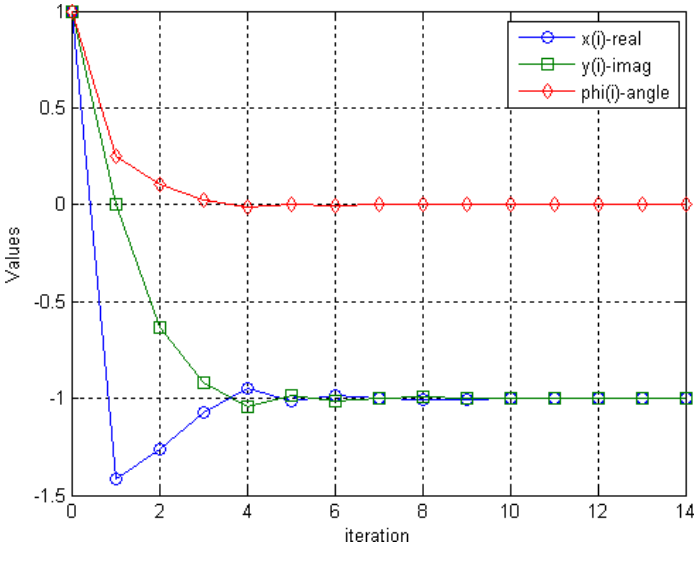

Fig. 11. Convergence curve of rotating mode (color online).

Figure 12 shows the performance of MIMO-OFDM detection with the JQRPSD. The radius size at each stage of the sphere decoder is[15]: $R = 2K\sigma^2 N_R$, $N_R \in [Nr, Nr-1, Nr-2, \ldots, 1]$ where K is the crucial factor of the radius constraint to select, sigma is noise variance, and N_R denotes the number of received antennas. The

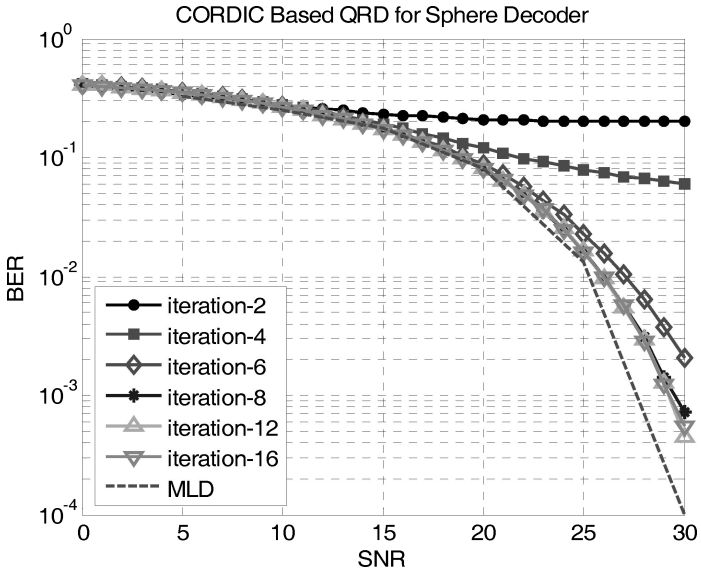

Fig. 12. Performance of MIMO-OFDM detection with the JQRPSD for different iterations of CORDIC computing.

uncoded bit error rate (BER) floating-point simulation result is produced by the QR decomposition based on CORDIC with different iterations in 64-QAM and 4×4 MIMO system. The Rayleigh fading and AWGN channel are employed for all curve simulations in Fig. 12, and the curves of 8 to 16 iterations are extremely similar. The channel response is assumed to be an ideal estimation in the simulation. For practical system application, eight iterations of CORDIC computing for executing the QR decomposition are adequate to ensure input data accuracy in MIMO-OFDM detection. Table 1 lists additional simulation parameter information.

This study performs fixed-point simulation to determine the most favorable number of bits for hardware implementation. Figure 13 shows the mean square error (MSE) versus wordlength at eight iterations. The MSE represents the error between the fixed-point and floating-point QR decomposition output. In Fig. 13, the curve is

Table 1. Simulation parameter information.

Parameter	Value
Bandwidth	20 MHz
Number of sub-carriers (N_c)	64 (64 FFT)
Useful symbol duration	3.2 μs
Guard time	0.6 μs
Modulation	64-QAM

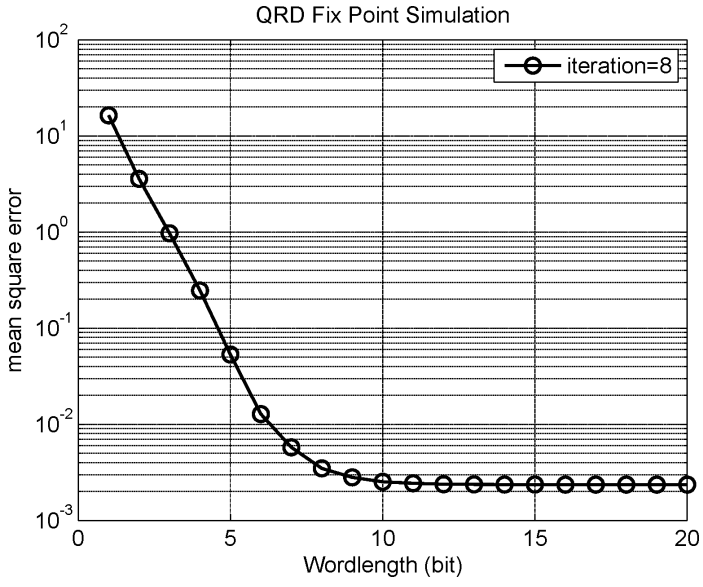

Fig. 13. Fixed-point simulation of QR decomposition with different word lengths.

saturated with 10-3 MSE. Increasing the number of bits does not affect system performance. Therefore, an 8-bit wordlength is sufficient in this system.

Table 2 illustrates the comparison results of this study with the folding structure [9] and Gram−Schmidt algorithm.[10,11] Although the folding structure has a similar gate count to that of the RQRD structure, the memory required is 4 times greater and the clock latency is more than that of the proposed structure. As Table 2 shows, the proposed architecture has lower clock latency and a smaller hardware area (gate count) than does the TSA structure. Compared with the Gram−Schmidt approach, it reduces gate count at the same matrix order by 64%. The vectoring hardware A_{Vec} and rotating hardware A_{Rot} are approximately equal to 3.5 k gate counts, and the required memory for this RQRD architecture is defined as $m^2 \times p$.

Table 2. Comparision of the QR decomposition implementation results.

	This work Givens rotation		Ref. 9	Ref. 10	Ref. 11
Algorithm	TSA	RQRD	Givens rotation	Gram−Schmidt	Gram−Schmidt
Order	8 × 8 (real)	8 × 8 (real)	4 × 4 (complex)	4 × 4 (real)	8 × 8 (real)
Iteration	8	8	8	None	None
Clock latency	448	240	252	67	152
Technology	0.18-μm CMOS	0.18-μm CMOS	FPGA	0.18-μm CMOS	0.18-μm CMOS
Gate count	128 k	32 k	1528 LC	72 k	77 k
Memory	None	None	2416 bits	None	None

6. Conclusion

This paper presents a modified implementation of QR decomposition, based on the Givens rotation method for a MIMO-OFDM detection system in a wireless baseband receiver. The CORDIC architecture for the RQRD can efficiently reduce the hardware cost for wireless MIMO-OFDM detection systems because the CORDIC architecture with vectoring and rotating modes requires no multiplications. The QR decomposition schedule of operation reduces clock latency and improves precision of detection performance. The proposed architecture is implemented and verified using TSMC 0.18 μm CMOS technology in the Rayleigh fading and AWGN, where the CORDIC is constructed by the 8-bit word length and 8-time iteration. The proposed RQRD architecture has a smaller hardware area than do the TSA and Gram−Schmidt architectures and can effectively reduce clock latency by 46%, as compared to using the TSA architecture.

Acknowledgments

This work was supported in part by the National Science Council (NSC), Taiwan, R.O.C. under Grant NSC 101-2220-E-005-001 and NSC 101-2220-E-167-001 and in part by the Ministry of Education, Taiwan, under the Aim for the Top University Plan. The authors would like to thank the National Chip Implementation Center of Taiwan for the technical support.

References

1. K. Nishimori, N. Honma, T. Seki and K. Hiraga, On the transmission method for short-range MIMO communication, *IEEE Trans. Vehic. Tech.* **60** (2011) 1247−1251.
2. C. I. Votis, P. Kostarakis and L. P. Ivrissimtzis, Design and measurements of a multiple-output transmitter for MIMO applications, *J. Circuits Syst. Comput.* **20** (2011) 515−529, doi:10.1142/S0218126611007426.
3. R. C. Daniels, C. M. Caramanis and R. W. Heath, Adaptation in convolutionally coded MIMO-OFDM wireless systems through supervised learning and SNR ordering, *IEEE Trans. Vehic. Tech.* **59** (2010) 114−126.
4. C. I. Votis, P. Kostarakis and L. P. Ivrissimtzis, Design and measurements of a multiple-output transmitter for MIMO applications, *J. Circuits Syst. Comput.* **20** (2011) 515−529, doi: 10.1142/S0218126611007426.
5. L. Xu, D. Xu, X. Zhang, S. Xu, J. Wang and Y. Li, Dynamic resource allocation with finite rate feedback for multiuser MIMO-OFDM systems, *J. Circuits Syst. Comput.* **20** (2011) 501−513, doi:10.1142/S0218126611007414.
6. P. Rabiei, W. Namgoong and N. Al-Dhahir, Reduced-complexity joint baseband compensation of phase noise and I/Q imbalance for MIMO-OFDM systems, *IEEE Trans. Wireless Commun.* **9** (2010) 3450−3460.
7. Y. Jung, S. Lee and J. Kim, Design and implementation of symbol detector for MIMO spatial multiplexing systems, *J. Circuits Syst. Comput.* **20** (2011) 727−739, doi: 10.1142/S0218126611007578.

8. K.-C. Lai and L.-W. Lin, Low-complexity adaptive tree search algorithm for MIMO detection, *IEEE Trans. Wireless Commun.* **8** (2009) 3716−3726.
9. F. Sobhanmanesh and S. Nooshabadi, Parametric minimum hardware QR-factoriser architecture for V-BLAST detection, *IEE Proc. Circuits Dev. Syst.* **153** (2006) 433−441.
10. C. K. Singh, S. H. Prasad and P. T. Balsara, VLSI architecture for matrix inversion using modified Gram-Schmidt based QR decomposition, *Proc. Int. Conf. VLSI Design* (2007), pp. 836−841.
11. K.-H. Lin, R. C.-H. Chang, H.-L. Lin and C.-F. Wu, Analysis and architecture design of a downlink M-modification MC-CDMA system using the Tomlinson-Harashima precoding technique, *IEEE Trans. Vehic. Tech.* **57** (2008) 1387−1397.
12. F. J. Jaime, M. A. Sanchez, J. Hormigo, J. Villalba and E. L. Zapata, Enhanced scaling-free CORDIC, *IEEE Trans. Circuits Syst. I: Reg. Papers* **57** (2010) 1654−1662.
13. P. K. Meher, J. Valls, T.-B. Juang, K. Sridharan and K. Maharatna, 50 years of CORDIC: Algorithms, architectures, and applications, *IEEE Trans. Circuits Syst. I: Reg. Papers* **56** (2009) 1893−1907.
14. C.-J. Ahn, Parallel detection algorithm using multiple QR decompositions with permuted channel matrix for SDM/OFDM, *IEEE Trans. Vehic. Tech.* **57** (2008) 2578−2582.
15. H.-L. Lin, H.-L. Chen and R. C. Chang, JQRPSD detection with low complexity for SDM MIMO wireless communication system, *Proc. Int. Symp. VLSI Design Automation Test (VLSI-DAT'07)* (2007).
16. S.-Fu Hsiao and J.-M. Delosme, Householder CORDIC algorithms, *IEEE Trans. Comput.* **44** (1995) 990−1001.
17. R. C.-H. Chang, C.-H. Lin, K.-H. Lin, C.-L. Huang and F.-C. Chen, Iterative QR decomposition architecture using the modified Gram-Schmidt algorithm for MIMO systems, *IEEE Trans. Circuits Syst. I: Reg. Papers* **57** (2010) 1095−1102.